ACS APPLIED NANO MATERIALS

www.acsanm.org Letter

Electrically Conductive Oxidation-Resistant Boron-Coated Carbon Nanotubes Derived from Atmospheric CO_2 for Use at High Temperature

Gi Mihn Kim, Won Yeong Choi, Jae Hyun Park, Seung Jin Jeong, Jong-Eun Hong, WooChul Jung, and Jae W. Lee*

Cite This: *ACS Appl. Nano Mater.* 2020, 3, 8592–8597 Read Online

ACCESS | Metrics & More | Article Recommendations | Supporting Information

ABSTRACT: This study introduces high-temperature antioxidative carbon nanotubes (CNTs) derived from carbon dioxide (CO_2). The individual CNT is coated by an amorphous boron layer that acts as a protection layer for carbon networks. It has a remarkable stability on thermal oxidation and provides a remarkable electrical conductivity of 4 S cm^{-1} at 1000 °C, while conventional carbon-based materials, including commercial CNTs, cannot maintain electrical properties because of oxidation below 400 °C. Thus, the novel atmospheric CO_2-based chemical vapor decomposition route can contribute to the applications of carbon-based material in high-temperature oxidation conditions such as a solid oxide fuel cell.

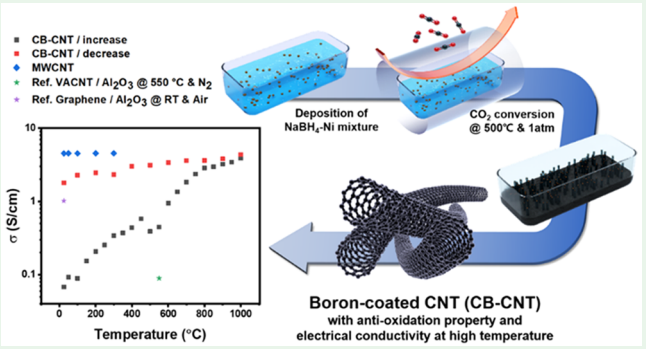

KEYWORDS: *boron-coated carbon nanotubes, CO_2 conversion, antioxidation, electrical conductivity, high temperature*

High-temperature applications require materials to retain various characteristics such as thermal stability, chemical and corrosion resistance, and good electrical conductivity at extreme conditions.[1,2] Therefore, it is not easy for conventional materials to satisfy all of the requirements. While single compounds of ceramics are widely used as solid oxide fuel cell (SOFC) electrode materials in the high-temperature conditions, they have a problem of exhibiting electrical conductivity only under a specific temperature range.[2,3]

To overcome the limitations of typical ceramics, the strategy of combining the ceramics with carbon materials has been suggested.[4,5] Among them, carbon nanotube (CNT)/ceramic composites are remarkable because of their good mechanical properties and electrical conductivity.[6] However, it is still difficult to apply the CNT/ceramic composites at high-temperature conditions because of low antioxidative capability, which is attributed to the combustion of carbon material[7] at temperatures higher than 500 °C. Recently, several methods to coat the inside and outside of CNTs with aluminum oxide (Al_2O_3) using atomic layer deposition[8] and laser-assisted chemical vapor deposition (CVD)[2] have been proposed. The main purpose of the integration of Al_2O_3 is to protect the CNTs, which are vulnerable to oxidation or combustion at high temperature. Both cases have succeeded in improving the antioxidative capability of CNT/ceramic composites, but they require more than two complex processes as additional steps for Al_2O_3 coating.

This study introduces a novel single-step method to synthesize a boron-coated CNT (CB-CNT), which has excellent thermal stability under high-temperature oxidation conditions. On the basis of the synthesis of boron-doped porous carbon[9−14] from gaseous carbon dioxide (CO_2), we demonstrate a novel CO_2-based CVD route to synthesize a CB-CNT from 1 bar of gaseous CO_2 at temperatures between 500 and 600 °C. The as-synthesized CB-CNT contains an exceptionally higher boron content at the surface than 30 atom %, and the coated boron is first oxidized at high temperature to become B_2O_3, which acts as a layer protecting the CNT from oxidation even up to 1000 °C. As a result, the unprecedented antioxidative CNT can be easily made by the one-step CO_2-based CVD route without the need for hybridization with other materials or additional complex steps. The structure of this CNT is analyzed in detail by electron microscopy, X-ray photoelectron spectroscopy (XPS), Raman spectroscopy, and electron energy loss spectroscopy (EELS). In addition, by measuring the electrical conductivity in situ under high-temperature oxidation conditions, we show for the first time

Received: July 15, 2020
Accepted: August 19, 2020
Published: August 19, 2020

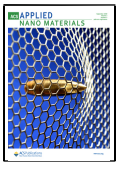

https://dx.doi.org/10.1021/acsanm.0c01909
ACS Appl. Nano Mater. 2020, 3, 8592–8597

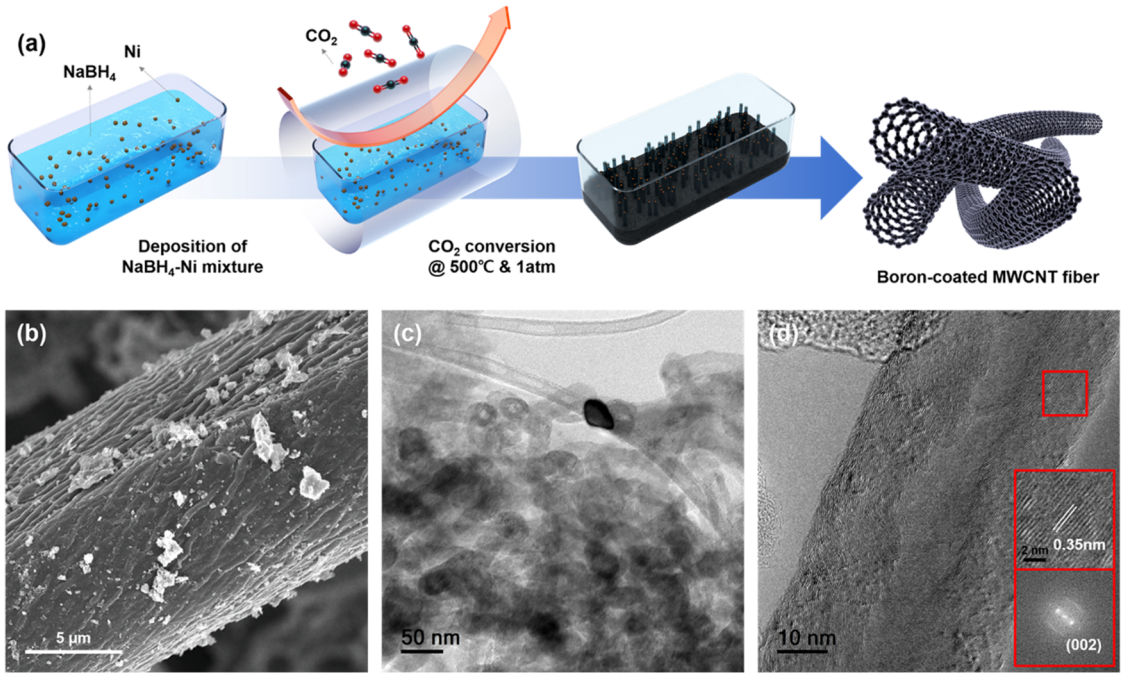

Figure 1. (a) Schematic illustration for the synthetic route of the CB-CNT based on CO_2-based CVD. (b) SEM image of the CB-CNT. (c) TEM image of the CB-CNT and (d) its high-magnification version [insets: FFT pattern and interlayer spacing of carbon (002)].

that the CO_2-derived CB-CNT can maintain electrical conductivity in the wide temperature range, revealing an excellent electrical conductivity of 3.89 S cm^{-1} at 1000 °C. As a result, we measured the electrical conductivity of the CB-CNT in oxidative conditions at high temperatures and verified that it was higher than those of CNT/ceramic and graphene/ceramic composites.[4,5] The oxidation resistance of the electrically conductive carbon material increases the applicability of the carbon, which has already been widely used in the energy storage field,[15,16] to high-temperature applications such as a SOFC.

The one-step preparation of CB-CNTs was achieved by employing sodium borohydride ($NaBH_4$) as a reduction agent and nickel(II) chloride ($NiCl_2$) as a precursor for nickel nanoparticles, as illustrated in Figure 1a. The origin of the synthesis of the CB-CNT is the deposition of methane, which is the product of reduction of CO_2 by a reducing agent,[17] onto nickel particles based on in situ gas analyses on the real-time synthesis process (Figure S1).

The scanning electron microscopy (SEM) image indicated that the CB-CNT developed CNT fibers (Figure 1b). It stretched from 150 μm to 1.88 mm in length, and its diameter ranged from 7.5 to 16 μm (Figure S2). The CB-CNT had a bundle of smaller fibers, and the fibers were highly populated (Figure 1b,c). The CB-CNT fibers were suspended in ethanol and sonicated for about 1 h to investigate an individual CNT by separating it from the fibers before the transmission electron microscopy (TEM) observations. The individual CNT was present in the form of a multiwalled carbon nanotube (MWCNT), which had more than 20 walls (Figure 1d). The fast Fourier transform (FFT) pattern on the wall showed the typical properties of a MWCNT with crystallinity in the (002) direction and an interlayer distance between (002) planes of 0.35 nm (insets of Figure 1d).[18]

XPS is performed to investigate the surface elemental composition of the CB-CNT, as listed in Table 1 and Figure S3 and Tables S1 and S2. According to the XPS survey results, the CB-CNT contained an amount of boron close to 30 atom % (Table 1 and Figure S3a). This content is exceptionally high compared to previous studies that showed 2.07−7.87% of doped boron (a detailed comparison is listed in Table S3).[19−23] In fact, among the peaks obtained by deconvoluting the high-resolution spectra for C 1s, the C−B bonding peak was found at around 283.8 eV[24] (Figure S3b). Moreover, the spectra for B 1s indicated that the boron exists in the form of C−B bonding, not in an elemental form, based on several peaks, such as B_4C (~187.8 eV), BC_3 (~189.3 eV), and BCO_2 (~192.5 eV) (Figure S3c).[25] Specifically, B_4C is the dominant C−B bonding in the CB-CNT (Tables S1 and S2).

Table 1. Summary of the Surface Elemental Composition of the CB-CNT Based on the XPS Survey Results[a]

sample	C 1s (atom %)	O 1s (atom %)	B 1s (atom %)
CB-CNT	49.29 (2.80)	16.96 (0.37)	33.75 (3.54)
CB-CNT (after oxidation at 900 °C)	15.80 (3.05)	64.69 (2.50)	19.51 (0.60)

[a]The standard deviation (SD) is in parentheses.

To confirm where 30 atom % boron exists in the CB-CNT, a high-resolution TEM (HRTEM) image was obtained, as shown in Figure 2a, and an amorphous layer was found outside the graphene layer. The composition of this amorphous layer was verified by EELS by a line scanning perpendicular to the individual CNT axis (Figure 2b). At the line profiling of carbon and boron for each location (Figure 2c), the carbon was distributed along with the tube, but the distribution of boron was quite remarkable because the signal indicated that the boron was distributed along the outer surface of the CNT as in the carbon coated with boron, which indicates that the amorphous layer in the HRTEM image is related to the boron. Such results allowed us to surmise that

https://dx.doi.org/10.1021/acsanm.0c01909
ACS Appl. Nano Mater. 2020, 3, 8592−8597

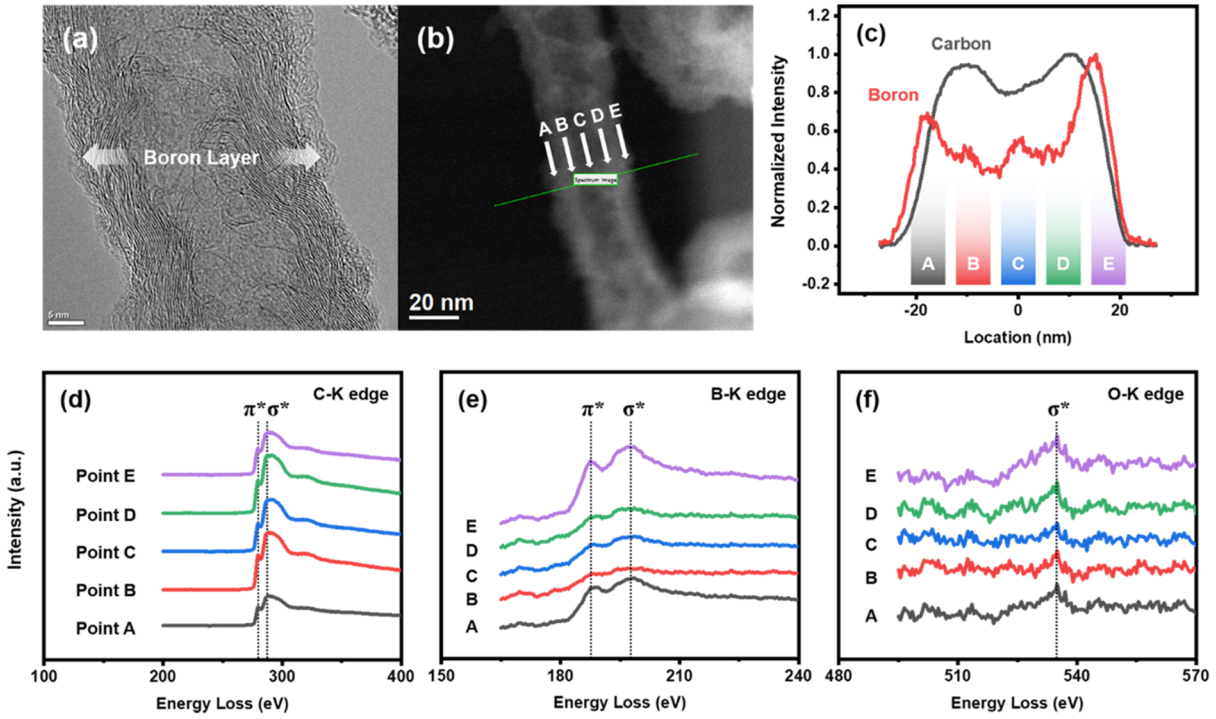

Figure 2. (a) HRTEM image. (b) Scanning TEM image of the CB-CNT to obtain the EELS spectra (the green line indicates the location for the EELS line profiling). (c) Overlay of the carbon and boron signals from the EELS line profiling depending on the location. (d–f) EELS spectra of each element depending on the location.

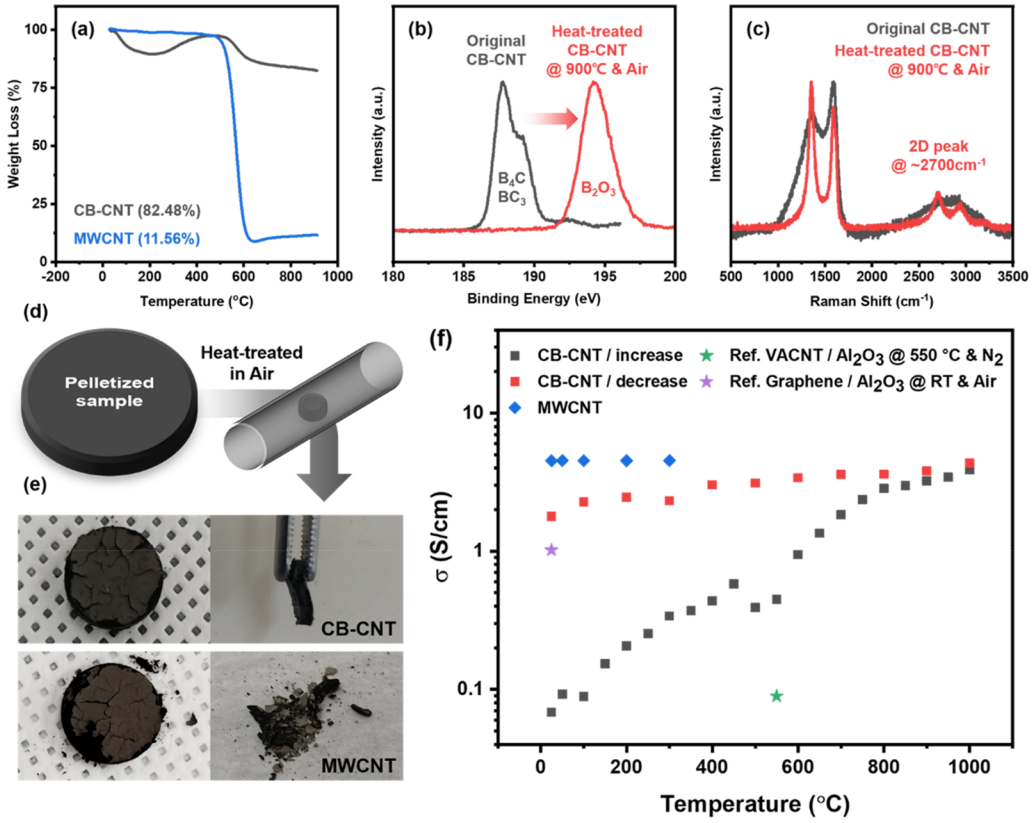

Figure 3. (a) TGA plots of the CB-CNT and commercial MWCNT in air. (b) Comparison of B 1s plots between the CB-CNT and its residue after oxidation up to 900 °C. (c) Comparison of the Raman spectra between the CB-CNT and its residue after oxidation up to 900 °C. (d) Schematic diagram for the experiment to measure the electrical conductivity of the sample under high-temperature oxidation. (e) Comparison of the state of pellets between the CB-CNT and MWCNT after measurement up to 900 °C. (f) Calculated electrical conductivity depending on the temperature (the error bars and a detailed determination for the CB-CNT data are shown in Figure S5).

https://dx.doi.org/10.1021/acsanm.0c01909
ACS Appl. Nano Mater. 2020, 3, 8592–8597

the CB-CNT was produced from CO_2 via the $NaBH_4$-based CVD method. This coated boron can contribute to the high amount of boron that was detected in the XPS survey results of the CB-CNT, and its bonding type in the interface between the graphene and amorphous boron layers is likely to be a hybrid of B_4C and BC_3, as confirmed by the deconvoluted B 1s spectra of XPS (Figure S3c). In addition, the EELS spectra for boron (Figure 2e) supported the existence of B_4C and BC_3 by showing that the well-developed π^* and σ^* peaks were observed only in the interface (marked as A and E in Figure 2e), while the π^* and σ^* peaks in the C−K edge were observed throughout the profiling line (Figure 2d). In BCO_2, it can be negligible because there was a very weak signal for the oxygen atom without the developed type of π^* and σ^* peaks in the EELS line profiling (Figure 2f).

We performed thermogravimetric analysis (TGA) to elucidate the thermal and antioxidative properties of the CB-CNT. The thermal oxidation behavior of the CB-CNT is distinctly different from that of the conventional carbon materials, as shown in Figure 3a. In general, amorphous carbon decomposes at 300−400 °C, and crystalline carbon, including graphene and CNTs, decomposes at about 500 °C in an oxidizing atmosphere. As a result, both of the carbon materials disappear above 800 °C and show near zero weight,[7,26] as verified in the case of the commercial MWCNT (the blue plot in Figure 3a). However, the CB-CNT remains over 80% even after 900 °C, which is the highest retention rate in CNT-based materials[8] (~36%), including graphene[5] (under 10%) measured by TGA for antioxidative capability in air.

To investigate the origin of the unusual thermal oxidation stability revealed in TGA, we performed XPS analysis on the residue from the CB-CNT after thermal oxidation up to 900 °C. There was approximately 15 atom % carbon (Table 1), which meant that the carbon networks were preserved under high-temperature oxidation. Interestingly, the state of boron changed from B_4C, BC_3, and BCO_2 (the black line in Figure 3b) to boron oxide close to B_2O_3 based on the B 1s graphs and a binding energy of about 194 eV (the red line in Figure 3b).[27] This result suggested that the boron coating can affect the unique behavior of the superior antioxidative capability. The rich boron covering the CNT would oxidize at 200 °C and become boron oxide (B_2O_3), which contributed to an increase in the mass of the CB-CNT due to the incorporated oxygen, as in the case of the coating on a diamond.[27] Then above 400 °C, the B_2O_3 layer protected the carbon atoms from thermal decomposition, but there was also decomposition of carbon atoms without the B_2O_3 layer, which reduced the mass after 400 °C in the TGA plot. As a result, the B_2O_3 layer acted as a protective layer to increase the stability of the carbon from thermal oxidation.[27] Therefore, the CB-CNT showed a retention of more than 80%. In particular, the protection system by the B_2O_3 layer worked effectively on the synthesized CNTs that were coated with boron. Raman analyses on the residues showed that the structure of the CNT was preserved well after thermal oxidation at 900 °C, based on the apparent D, G, and 2D bands (Figure 3c). In addition, because the amorphous carbon without the boron protection layer gasified, the Raman spectrum of the CB-CNT became close to that of pure MWCNTs, which had sharper and more intensified bands than the original CB-CNT (the red line in Figure 3c).[28] The SEM image of the residue supports the existence of CNTs by showing the preserved CNT shape and the fiber shape (Figure S4). These outstanding thermal characteristics confirm that the CB-CNT can be applied to high-temperature oxidation conditions.

To ensure application of the CB-CNT to high-temperature oxidation conditions, the electrical conductivity depending upon the temperature ramping was obtained with four-probe current−voltage (I−V) curve measurement on pelletized CB-CNT in a furnace (Figure 3d), and it is summarized in Figure 3f. The CB-CNT at room temperature had a lower electrical conductivity than the commercial MWCNT because the CB-CNT had a large amount of boron and oxygen (ca. 50 atom % in Table 1), which were less electrically conductive than the pure CNTs.[2] Above 400 °C, the MWCNT began to decompose, so the pellet collapsed (Figure 3e), and measurement was impossible. With the CB-CNT, however, the B_2O_3 layer protected most of the carbon networks, including the CNT. Therefore, the CB-CNT was able to maintain the electrical conductivity over 400 °C. At 550 °C, the conductivity of the CB-CNT in an air atmosphere reached 0.45 S cm^{-1}, which was superior to those of vertically aligned CNTs/Al_2O_3[2] (0.089 S cm^{-1} measured at 550 °C in nitrogen). After 450 °C, there was a decrease in the electrical conductivity, which we saw as the effect of the phase change of B_2O_3 because the temperature corresponded to its melting point. However, the CB-CNT became stable, and the electrical conductivity increased sharply. At 650 °C, the electrical conductivity of the CB-CNT exceeded 1.02 S cm^{-1} of graphene/Al_2O_3,[5] which was measured at room temperature. Consequently, it is remarkable that the CB-CNT provides stable electrical conductivity even at 1000 °C at about 4 S cm^{-1}. To the best of our knowledge, our study introduced for the first time the implementation and measurement of the electrical conductivity up to 1000 °C under oxidation environments for carbon-based composites. In addition, the CB-CNT demonstrated competitive electrical conductivity superior to other carbon/ceramic composites at high temperatures. After reaching 1000 °C in air, the temperature was maintained for 12 h at the same conditions to identify the thermal stability of the CB-CNT. Then, the electrical conductivity was measured while the temperature decreased in air (the red square in Figure 3f). While the electrical conductivity slightly decreased according to the temperature decrease, the CB-CNT still maintained a high electrical conductivity of 1.7 S cm^{-1} when it returned to room temperature. Typical high-temperature electrochemical applications, SOFC and protonic ceramic fuel cell (PCFC), require electrode materials (SOFC, anode; PCFC, cathode) to have more than 1 S cm^{-1} during the high-temperature operation.[29,30] As a result, the CB-CNT can meet the requirements, which indicates that the CB-CNTs have the potential to be used as electrode materials in high-temperature electrochemical devices.

We have synthesized CB-CNTs with a high boron amount of 30% using CO_2 as the carbon source. Because the boron coating layer acted as a protective layer of carbon atoms against thermal oxidation first by oxidizing to become B_2O_3, and the CB-CNT endured above 900 °C. Therefore, the CB-CNT represents a competitive electrical conductivity even up to 1000 °C (ca. 4 S cm^{-1}). This unique high-temperature stability confirmed that carbon-based materials can be applied to high-temperature oxidation environments including the SOFC.

https://dx.doi.org/10.1021/acsanm.0c01909
ACS Appl. Nano Mater. 2020, 3, 8592−8597

■ ASSOCIATED CONTENT

Supporting Information

The Supporting Information is available free of charge at https://pubs.acs.org/doi/10.1021/acsanm.0c01909.

Experimental sections, including preparation and characterization of the CB-CNT and conductivity measurements, supporting figures, including the synthesis mechanism of CB-CNT, and supporting tables (PDF)

■ AUTHOR INFORMATION

Corresponding Author

Jae W. Lee − *Department of Chemical and Biomolecular Engineering, Korea Advanced Institute of Science and Technology, Daejeon 34141, Republic of Korea;* orcid.org/0000-0002-8756-0195; Email: jaewlee@kaist.ac.kr

Authors

Gi Mihn Kim − *Department of Chemical and Biomolecular Engineering, Korea Advanced Institute of Science and Technology, Daejeon 34141, Republic of Korea*

Won Yeong Choi − *Department of Chemical and Biomolecular Engineering, Korea Advanced Institute of Science and Technology, Daejeon 34141, Republic of Korea*

Jae Hyun Park − *Department of Chemical and Biomolecular Engineering, Korea Advanced Institute of Science and Technology, Daejeon 34141, Republic of Korea*

Seung Jin Jeong − *Department of Materials Science and Engineering, Korea Advanced Institute of Science and Technology, Daejeon 34141, Republic of Korea;* orcid.org/0000-0001-6125-6833

Jong-Eun Hong − *Fuel Cell Laboratory, Korea Institute of Energy Research, Daejeon 34129, Republic of Korea*

WooChul Jung − *Department of Materials Science and Engineering, Korea Advanced Institute of Science and Technology, Daejeon 34141, Republic of Korea;* orcid.org/0000-0001-5266-3795

Complete contact information is available at: https://pubs.acs.org/10.1021/acsanm.0c01909

Notes

The authors declare no competing financial interest.

■ ACKNOWLEDGMENTS

The authors acknowledge support from the Korea CCS R&D Center and Energy Clouds program funded by the Ministry of Science and ICT (Grants NRF-2014M1A8A1049297 and NRF-2019M3F2A1072237).

■ REFERENCES

(1) Tamalampudi, S. R.; Patole, S.; Alfakes, B.; Sankar, R.; Almansouri, I.; Chiesa, M.; Lu, J.-Y. High-Temperature Defect-Induced Hopping Conduction in Multilayered Germanium Sulfide for Optoelectronic Applications in Harsh Environments. *ACS Appl. Nano Mater.* **2019**, *2* (4), 2169−2175.

(2) Zou, Q. M.; Deng, L. M.; Li, D. W.; Zhou, Y. S.; Golgir, H. R.; Keramatnejad, K.; Fan, L. S.; Jiang, L.; Silvain, J. F.; Lu, Y. F. Thermally Stable and Electrically Conductive, Vertically Aligned Carbon Nanotube/Silicon Infiltrated Composite Structures for High-Temperature Electrodes. *ACS Appl. Mater. Interfaces* **2017**, *9* (42), 37340−37349.

(3) Damm, D. L.; Fedorov, A. G. Radiation heat transfer in SOFC materials and components. *J. Power Sources* **2005**, *143* (1−2), 158−165.

(4) Picot, O. T.; Rocha, V. G.; Ferraro, C.; Ni, N.; D'Elia, E.; Meille, S.; Chevalier, J.; Saunders, T.; Peijs, T.; Reece, M. J.; Saiz, E. Using graphene networks to build bioinspired self-monitoring ceramics. *Nat. Commun.* **2017**, *8*, 14425−14435.

(5) Zhang, Q. Q.; Lin, D.; Deng, B. W.; Xu, X.; Nian, Q.; Jin, S. Y.; Leedy, K. D.; Li, H.; Cheng, G. J. Flyweight, Superelastic, Electrically Conductive, and Flame-Retardant 3D Multi-Nanolayer Graphene/Ceramic Metamaterial. *Adv. Mater.* **2017**, *29* (28), 1605506−1605517.

(6) Curtin, W. A.; Sheldon, B. W. CNT-reinforced ceramics and metals. *Mater. Today* **2004**, *7* (11), 44−49.

(7) Lehman, J. H.; Terrones, M.; Mansfield, E.; Hurst, K. E.; Meunier, V. Evaluating the characteristics of multiwall carbon nanotubes. *Carbon* **2011**, *49* (8), 2581−2602.

(8) Stano, K. L.; Carroll, M.; Padbury, R.; McCord, M.; Jur, J. S.; Bradford, P. D. Conformal Atomic Layer Deposition of Alumina on Millimeter Tall, Vertically-Aligned Carbon Nanotube Arrays. *ACS Appl. Mater. Interfaces* **2014**, *6* (21), 19135−19143.

(9) Zhang, J. S.; Lee, J. W. Production of boron-doped porous carbon by the reaction of carbon dioxide with sodium borohydride at atmospheric pressure. *Carbon* **2013**, *53*, 216−221.

(10) Kim, Y. K.; Park, J. H.; Lee, J. W. Facile nano-templated CO2 conversion into highly interconnected hierarchical porous carbon for high-performance supercapacitor electrodes. *Carbon* **2018**, *126*, 215−224.

(11) Byeon, A.; Park, J.; Baik, S.; Jung, Y.; Lee, J. W. Effects of boron oxidation state on electrocatalytic activity of carbons synthesized from CO2. *J. Mater. Chem. A* **2015**, *3* (11), 5843−5849.

(12) Zhang, J. S.; Byeon, A.; Lee, J. W. Boron-doped electrocatalysts derived from carbon dioxide. *J. Mater. Chem. A* **2013**, *1* (30), 8665−8671.

(13) Baik, S.; Suh, B. L.; Byeon, A.; Kim, J.; Lee, J. W. In-situ boron and nitrogen doping in flue gas derived carbon materials for enhanced oxygen reduction reaction. *J. CO2 Util.* **2017**, *20*, 73−80.

(14) Byeon, A.; Baik, S.; Lee, J. W. Enhanced electrocatalytic reduction of oxygen at CO2-derived Fe-N-B-doped porous carbon. *J. CO2 Util.* **2018**, *26*, 28−35.

(15) Wang, J.; Xu, Y.; Ding, B.; Chang, Z.; Zhang, X.; Yamauchi, Y.; Wu, K. C. Confined Self-Assembly in Two-Dimensional Interlayer Space: Monolayered Mesoporous Carbon Nanosheets with In-Plane Orderly Arranged Mesopores and a Highly Graphitized Framework. *Angew. Chem. Int. Ed.* **2018**, *57* (11), 2894−2898.

(16) Dutta, S.; Kim, J.; Ide, Y.; Ho Kim, J.; Hossain, M. S. A.; Bando, Y.; Yamauchi, Y.; Wu, K. C. W. 3D network of cellulose-based energy storage devices and related emerging applications. *Mater. Horiz.* **2017**, *4* (4), 522−545.

(17) Kim, G. M.; Lim, W.-G.; Kang, D.; Park, J. H.; Lee, H.; Lee, J.; Lee, J. W. Transformation of Carbon Dioxide into Carbon Nanotubes for Enhanced Ion Transport and Energy Storage. *Nanoscale* **2020**, *12* (14), 7822−7833.

(18) Eom, S.; Cho, S. H.; Goto, T.; Chun, M. P.; Sekino, T. Low-Dimensional Carbon and Titania Nanotube Composites via a Solution Chemical Process and Their Nanostructural and Electrical Properties for Electrochemical Devices. *ACS Appl. Nano Mater.* **2019**, *2* (10), 6230−6237.

(19) Sheng, Z. H.; Gao, H. L.; Bao, W. J.; Wang, F. B.; Xia, X. H. Synthesis of boron doped graphene for oxygen reduction reaction in fuel cells. *J. Mater. Chem.* **2012**, *22* (2), 390−395.

(20) Yu, X. M.; Han, P.; Wei, Z. X.; Huang, L. S.; Gu, Z. X.; Peng, S. J.; Ma, J. M.; Zheng, G. F. Boron-Doped Graphene for Electrocatalytic N-2 Reduction. *Joule* **2018**, *2* (8), 1610−1622.

(21) Van Tam, T.; Kang, S. G.; Babu, K. F.; Oh, E. S.; Lee, S. G.; Choi, W. M. Synthesis of B-doped graphene quantum dots as a metal-free electrocatalyst for the oxygen reduction reaction. *J. Mater. Chem. A* **2017**, *5* (21), 10537−10543.

(22) Yeh, M.-H.; Leu, Y.-A.; Chiang, W.-H.; Li, Y.-S.; Chen, G.-L.; Li, T.-J.; Chang, L.-Y.; Lin, L.-Y.; Lin, J.-J.; Ho, K.-C. Boron-doped carbon nanotubes as metal-free electrocatalyst for dye-sensitized solar

cells: Heteroatom doping level effect on tri-iodide reduction reaction. *J. Power Sources* **2018**, *375*, 29−36.
(23) Kang, D.; Lee, J. W. Enhanced methane decomposition over nickel-carbon-B2O3 core-shell catalysts derived from carbon dioxide. *Appl. Catal. B-Environ.* **2016**, *186*, 41−55.
(24) Camisasca, A.; Sacco, A.; Brescia, R.; Giordani, S. Boron/Nitrogen-Codoped Carbon Nano-Onion Electrocatalysts for the Oxygen Reduction Reaction. *ACS Appl. Nano Mater.* **2018**, *1* (10), 5763−5773.
(25) Shen, W.; Li, H.; Wang, C.; Li, Z. H.; Xu, Q. J.; Liu, H. M.; Wang, Y. G. Improved electrochemical performance of the Na3V2-(PO4)3 cathode by B-doping of the carbon coating layer for sodium-ion batteries. *J. Mater. Chem. A* **2015**, *3* (29), 15190−15201.
(26) Bom, D.; Andrews, R.; Jacques, D.; Anthony, J.; Chen, B. L.; Meier, M. S.; Selegue, J. P. Thermogravimetric analysis of the oxidation of multiwalled carbon nanotubes: Evidence for the role of defect sites in carbon nanotube chemistry. *Nano Lett.* **2002**, *2* (6), 615−619.
(27) Sun, Y. H.; Meng, Q. N.; Qian, M.; Liu, B. C.; Gao, K.; Ma, Y. L.; Wen, M.; Zheng, W. T. Enhancement of oxidation resistance via a self-healing boron carbide coating on diamond particles. *Sci. Rep.* **2016**, *6*, 20198−20208.
(28) Hu, G. J.; Sun, Z. H.; Shi, C.; Fang, R. P.; Chen, J.; Hou, P. X.; Liu, C.; Cheng, H. M.; Li, F. A Sulfur-Rich Copolymer@CNT Hybrid Cathode with Dual-Confinement of Polysulfides for High-Performance Lithium-Sulfur Batteries. *Adv. Mater.* **2017**, *29* (11), 1603835−1603840.
(29) Atkinson, A.; Barnett, S.; Gorte, R. J.; Irvine, J. T. S.; McEvoy, A. J.; Mogensen, M.; Singhal, S. C.; Vohs, J. Advanced anodes for high-temperature fuel cells. *Nat. Mater.* **2004**, *3* (1), 17−27.
(30) Rioja-Monllor, L.; Bernuy-Lopez, C.; Fontaine, M.-L.; Grande, T.; Einarsrud, M.-A. Processing of high performance composite cathodes for protonic ceramic fuel cells by exsolution. *J. Mater. Chem. A* **2019**, *7* (14), 8609−8619.

https://dx.doi.org/10.1021/acsanm.0c01909
ACS Appl. Nano Mater. 2020, 3, 8592−8597